Title

SOME USES AND CHARACTERISTICS OP MOS TRANSISTORS FOR HEALTH PHYSICS APPLICATIONS

Author

McCaslin, Joseph B.

Publication Date

1965-07-01

UCRL-16446

University of California

Ernest O. Lawrence Radiation Laboratory

SOME USES AND CHARACTERISTICS OF
MOS TRANSISTORS FOR HEALTH PHYSICS APPLICATIONS

Berkeley, California

UCRL-16446
Errata

UNIVERSITY OF CALIFORNIA

Lawrence Radiation Laboratory
Berkeley, California

AEC Contract No. W-7405-eng-48

November 10, 1965

ERRATA

TO: All recipients of UCRL-16446

FROM: Technical Information Division

Subject: UCRL-16446, "Some Uses and Characteristics of MOS Transistors For Health Physics Applications," Joseph B. McCaslin, July 1965.

Please make to following corrections on subject report.

Page 1, paragraph 5, line 2 reads: "of a p-n function". It should read "of a p-n junction".

Page 2, paragraph 3, line 5 reads: "10^{-16} A". It should read "10^{-15} A".

Page 6. Please substitute enclosed page -6- for one now in report.

Page 16, Fig. 4, second from bottom 20 K should read 200 K, please [illegible] substitute enclosed page.

Scintillator-photomultiplier systems must be used with caution for radiation survey work near machines that have stray magnetic fields. The extent to which these fields interfere with survey measurements depends on the magnitude of the field, the orientation of the photomultiplier with respect to the field, and the effectiveness of whatever magnetic shielding surrounds the photomultiplier. It is always a risk to use photomultiplier tubes for measurements in magnetic fields. Count rates will be suppressed, and if one is accepting counts only in a narrow region of pulse heights, the possibility of losing counts is greatly enhanced.

Table 1. Pulse width relative to maximum amplitude.

Fraction of maximum pulse height	Pulse width (nsec)
1	30
3/4	45
1/2	60
1/4	80

Some measurements of rise time, pulse height, and duration were made using a high-frequency silicon transistor (2N2905) in a common base configuration. This type of circuit offers a low input impedance (25 to 50 ohms) and a current gain less than unity. Voltage gain depends on the value of the collector load resistor (R_L). However, rise time and pulse duration also depend on R_L. When R_L is chosen to be 10 kΩ the voltage gain is unity and the pulse rise and duration times are 100 and 200 nsec respectively. If R_L is chosen to be 1 kΩ, these times are 20 and 100 nsec; at 100 Ω they are 10 and 40 nsec. The voltage gain in the latter case is about 0.1.

If the signal from the Anton 805 is fed through a high voltage decoupling capacitor directly into a short length (2 ft) of RG/58-U and terminated at both ends by 50 Ω resistors, then the rise times appear to be $\leq$ 5 nsec and the pulse duration at half-maximum amplitude is 5 to 10 nsec. Maximum pulse height is only 0.08 of the height observed when high-impedance (100 kΩ) loads are used.

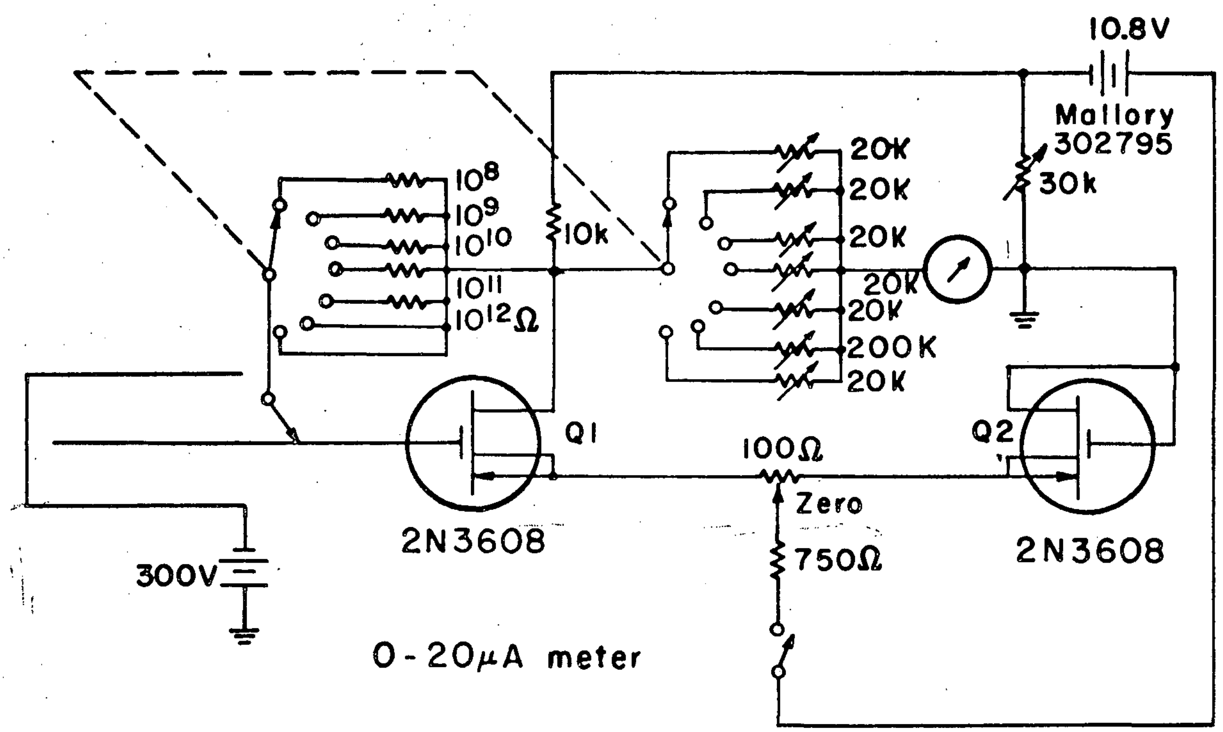

MUB-8369

Fig. 4

1st Symposium on Accelerator Radiation Dosimetry
and Experience, Brookhaven National Laboratory, Nov. 3-5, 1965
To be published in Proceedings

UCRL-16446

UNIVERSITY OF CALIFORNIA

Lawrence Radiation Laboratory
Berkeley, California

AEC Contract No. W-7405-eng-48

SOME USES AND CHARACTERISTICS OF MOS TRANSISTORS FOR HEALTH PHYSICS APPLICATIONS

Joseph B. McCaslin

July 1965

SOME USES AND CHARACTERISTICS OF MOS TRANSISTORS FOR HEALTH PHYSICS APPLICATIONS

Joseph B. McCaslin

Lawrence Radiation Laboratory
University of California
Berkeley, California

July 1965

ABSTRACT

Since 1963 the Health Physics Department at Lawrence Radiation Laboratory, Berkeley, has studied some of the characteristics of metal-oxide-semiconductor field-effect transistors (MOS), which may be useful in problems of radiation detection.

It has been found that these transistors are particularly suitable for electrometer applications. Input leakage currents of $\approx 10^{-16}$ A and transconductances of 750 μmhos are typical. Semiguarded MOS's exhibit leakage currents near 10^{-18} A, but the transconductance is down to about 70 μmhos.

These compare favorably with portable vacuum-tube electrometers, which may have leakage currents of 10^{-14} A and 200 μmhos transconductance when triode-connected, and 10^{-15} A and 20 μmhos when pentode-connected. Dynamic capacitor electrometers have drift rates that correspond to input leakage currents of 10^{-17} to 10^{-18} A.

Two portable MOS air ionization-chamber instruments have been constructed and have been in operation for more than one year. One is both an integrating type with a full-scale sensitivity of 1 μR, and a rate meter with ranges from 1 mR/h to 1 R/h; the other instrument is a rate meter only with ranges from 20 mR/h to 200 R/h.

The MOS, unlike its vacuum-tube counterpart, is a high-frequency device which is capable of operation in the nanosecond region. A fast BF_3 detector, pulse shaper, and line driver have been constructed which produces pulses of 30 to 80 ns duration at half-maximum pulse height. This moderated BF_3 system has been useful for fast-neutron monitoring at the Bevatron during rapid beam extraction. The sensitivity is 2 counts/n-cm^2.

A 4π anticoincidence G-M foil counter was constructed with MOS's in digital circuitry. The saturated zero-time sensitivity for 2-in.-diam. 2-g indium foils is 21 counts/min per n/cm^2-sec. Background with 2 in. of lead is 21 counts/min.

Static radiation damage tests were made in order to determine the suitability of MOS's in areas of high-level radiation such as target areas. Tests were performed with 7.5-MeV electrons in the range of absorbed dose from 10^4 through 10^8 rads, 7.5-MeV bremsstrahlung gammas at 10^6 rads, and an integrated thermal neutron exposure of 4×10^{14} n/cm^2. Data are presented that show postirradiation shifts in gate threshold voltage V_{GST}, dc transconductance g_m, drain-source leakage current I_{DSS}, and gate leakage current I_G. Effects of radiation on the drain-source and gate-source breakdown voltages are also given. The predominant effect of ionizing radiation on these devices is a gradual upward shifting of the gate threshold voltage such that at 10^8 rads the required bias is ≈ -15 V instead of the pre-irradiated value of -4.5 to -5 V. Gate input leakage current is considerably increased at 10^7 rads and is unpredictable at 10^8 rads. These tests indicate that MOS transistors, although superior in most respects to conventional vacuum-tube electrometers, are more easily damaged by large doses of ionizing radiation. They must be shielded when used in areas of sustained high radiation intensity.

SOME USES AND CHARACTERISTICS OF MOS TRANSISTORS FOR HEALTH PHYSICS APPLICATIONS

INTRODUCTION

Recent studies by the Health Physics group at Lawrence Radiation Laboratory, Berkeley, have shown that significant advantages can be realized by using MOS (metal-oxide-semiconductor) transistors in low-frequency electrometer applications.[1] (A summary of this work is presented along with some additions. Results of radiation-effects studies on these devices are also summarized.[2]) Radiation damage is an important consideration if MOS ionization chamber instruments are to be used to monitor high-level radiation areas.

MOS's are used also in two other applications. The first of these is a sensitive moderated fast BF_3 counter and associated linear circuitry, which shapes and transmits pulses of short duration over a 300-ft cable to a remote counting area. This system is used for resolving events during Bevatron rapid beam extraction (150 μsec). The second application involves MOS's in an anticoincidence arrangement with two pancake G-M counters in a 4π configuration. This portable low-current-drain system is intended for field measurements of moderated indium and gold foils.

These last two applications do not involve unique MOS characteristics in the sense that electrometer ionization chambers do. Rather, they illustrate other uses for these devices and point out some unusual, interesting, and useful characteristics.

MOS TRANSISTORS

The MOS transistor, also called the insulated-gate transistor, is unique in several respects. It performs well in low-frequency electrometer applications, and it can be used as an amplifier to hundreds of megacycles and as an oscillator to nearly 1 kMc. Its forward transfer characteristics resemble those of vacuum tubes (sharp-cutoff pentodes) rather than transistors. Enhancement-type MOS's can be used in direct-coupled stages without the need of bias-level-adjusting resistors.

Although the MOS is a field-effect transistor (FET), it does not depend on the reverse bias characteristics of a p-n function to obtain its high input impedance. In fact, when it is biased in its linear region the MOS has no diodes in series with the signal path, so that there is no offset voltage, and no rectification and detection of radio-frequency signals. The high dc input impedance of the MOS ($>10^{15}$ ohms for devices described here) is due to a thin layer of amorphous quartz located between the gate (signal input terminal) and the rest of the device.

Current flowing in the thin layer of silicon beneath the quartz is modulated by the electrostatic field applied at the gate. See Fig. 1. In vacuum-tube terms the gate, source, and drain are analogous to grid, cathode, and plate, respectively.

For a given semiconductor material four types of MOS transistors can be made. All are majority carrier devices and may be designed with either n or p channels. Both channel types can be designed to operate in either enhancement or depletion modes. Depletion-mode MOS's exhibit significant channel conduction with no external gate bias; enhancement-mode devices have essentially no source-to-drain conduction at zero bias.

Enhancement-mode p-channel transistors were used for the work described in this report.[3] Drain current, I_{DSS}, in these devices is only about 1 to 3 nA with zero gate-to-source voltage. This low value is due to the reverse-biased junction between the drain and the source-body terminals. When the gate-to-source voltage, V_{GS}, $\gtrsim$ -4.5 V the junction is effectively shunted by the channel, and the drain current increases. Negative charge carriers in the channel are repulsed by the electrostatic field of the gate and a p-type inversion layer or p channel is formed in that region. Forward biasing of the gate (making the gate more negative with respect to the source) causes enlargement of the cross-sectional area of the channel normal to the direction of current flow so that conduction is enhanced. The gate voltage conductivity-modulates the channel.

ELECTROMETER APPLICATIONS

Gate leakage current, I_G, was measured in 40 devices of the type (2N3608) used with the ion chambers. Figure 2 shows how I_G typically decreases with time following turn-on. It can be seen that the ultimate value of I_G will be approximately 1/7 to 1/10 of the value measured at 20 min. Of the 40 devices tested, two showed I_G's (20 min) less than 10^{-16} A. About half were between 1 and 2×10^{-15} A, one-third were between 2 and 6×10^{-15} A. Five devices were greater than 6×10^{-15} A, and the worst device showed a gate leakage of 3×10^{-13} A. I_G's for most of the devices are 1×10^{-16} A to 9×10^{-16} A after several hours.

Measurements of I_G were made with voltages and circuitry similar to those used in the integrating ion chamber. The relationship used was

$$I_G = \frac{C_i \, \Delta E_0}{G\, t} ,$$

where C_i = input capicitance corrected for Miller effect,
ΔE_0 = change in output voltage cause by a change in input voltage on the floating gate,
G = voltage gain of the device in the test circuit, and
t = time required for the output voltage to go from E_0 to $E_0 + \Delta E_0$.

The average transconductance, g_m, was 750 µmhos and was measured at I_D = 1 mA, $V_{GS} = V_{DS}$, with a 10-mV step applied to the gate. By contrast, typical pentode-connected vacuum-tube electrometers of the type used in portable instruments have g_m's of 10 to 20 µmhos and I_G's of about 10^{-15} A. Triode-connected tubes usually have g_m's ten times as high as pentodes, but also have I_G's about 10 or more times as high.

Gate-to-source leakage appears to be the dominant leakage mechanism in the 2N3608's. This is due to the spacing and voltage between gate lead and case, about 1/32 in. and -4.5 V. Measurements were made on a few MOS's (2N3610), which were somewhat guarded because the case may be connected to a guard potential equal to the gate-source potential. Short-term measurements showed I_G to be near 10^{-18} A. The direction of leakage could be changed by varying the guard potential a few millivolts from the optimum value. Both g_m (≈ 70 μmhos) and C_i are less than for the 2N3608's.

Figures 3 and 4 show a photograph and schematic diagram of the first of two MOS ion-chamber instruments. This was initially intended to be only an integrator. An unsealed 3700-cm^3 air ionization chamber was chosen so that in a background field of 10 μR/h the current would be ≈ 3×10^{-15} A. An integration time of 6 min would be required for the 1-μR/FS range (FS = full scale). The MOS leakage current of ≈ 10^{-16} A would not interfere greatly with this measurement.

The MOS forward transfer characteristic is linear over a large enough range of input voltages to allow for a second full-scale range of 10 μR by desensitizing the meter and allowing the input to integrate a larger voltage. However, a small amount of drift will occur for several minutes when the instrument is switched back to the 1-μR/FS range. Use of a larger integrating capacitor, instead of meter desensitizing for the 10-μR range, would prevent the drift.

Rate-meter ranges of 1 mR/h to 10 R/h were added. Full scale on the 1-mR/h range corresponds to an ion chamber current of ≈ 3×10^{-13} A with an input resistor of 10^{12} ohms. The time constant on this range is 11 sec.

Current drain from a single battery is only 0.7 mA, so that the instrument can be operated continuously for about 7 months. This adds greatly to stability and reduced leakage current. Only two transistors are used in a balanced amplifier circuit. Q_2 balances out temperature-induced fluctuations and it also circumvents the need for quiescent current bucking. Drift is not significant even over a period of several months.

Figure 5 shows the second MOS ion chamber instrument, which was made specifically for surveying the Bevatron vacuum ring during shutdown periods. These surveys must be made by a person crawling in dark and extremely cramped quarters. The finished instrument is small and lightweight, and has an illuminated meter. Rate-meter ranges are 20 mR/h to 200 R/h in decade steps. The circuitry is similar to the other instrument except that the gate of Q_2 is connected to the Q_1 drain so that the meter is arranged in push-pull fashion. The drain supply battery has been changed to 13.5 V, and the unsealed 125-cm^3 ion chamber has a collection potential of 180 V. The time constant on the 20-mR/h range is 8 sec.

Because both instruments have long time constants on the most sensitive range, the time required for the meter indicator to stabilize is much longer than expected if there are large switching transients. Very sensitive and stable low-cost ionization chamber instruments can be built using MOS transistors. Except for radiation-damage sensitivity (and this isn't a problem with portable survey instruments) MOS electrometers surpass the vacuum-tube variety in all important respects. Unguarded MOS electrometers can perform many Health Physics functions as well as can vibrating capacitor types, and in some respects (such as sensitivity to temperature change) they perform much better. Use of guarded or semi-guarded MOS's provides even further improvement.

FAST BF_3 COUNTER

The Bevatron beam can be spilled in 150 μsec under certain conditions. Fast-neutron measurements using conventional moderated BF_3 counters may contain large errors when the rapid beam extractor is used. If the duration of the BF_3 pulse is long compared with the spill time one may be counting little more than the repetition rate of the accelerator. Beam intensity, spill time, degree of BF_3 enrichment, size of counter, proximity of the counter to the source of neutrons, etc., are important in determining the maximum duration the BF_3 pulses may have if counting losses are to be kept small.

The approach used here is to shape the pulses from a sensitive BF_3 detector with linear circuitry in low-level stages so that pulse durations are made as short as possible. (See Fig. 6.) This system, when used with a suitable oscilloscope, makes it possible for one to decide if a significant number of counts are being lost. Use of B^{10}-depleted counters, Cd liners, distance, or a combination of these may be necessary to reduce the counting rate to an acceptable level. In any event, one needs a statistically significant number of short-duration BF_3 pulses and, in most cases, a system for driving these pulses with minimum loss and distortion to a remote area for counting.

BF_3 pulses are spread in time even with an instantaneous burst of neutrons. The mean life of neutrons in a volume of moderator such as we use is about 200 to 300 μsec, but the Cd liner, and boron in the detector, will reduce this to an estimated 100 μsec.[4] Experimental measurements of this time spread are planned for the near future.

It is possible, of course, to simply desensitize a counter so that counting losses are low. However, counting statistics suffer when this approach is used. For example, the Bevatron repetition rate is 10 ppm and the rapid beam spill is 150 μsec/pulse. If the BF_3 pulse pair resolution time is 5 μsec, a maximum of only 30 counts/pulse can be had, and under those conditions they would be meaningless because of counting losses. A less sensitive counter with the same resolving time could only yield statistically insignificant data. For this reason, we first attempt our measurements with high-sensitivity fast-counting systems. Only then is the detector desensitized if necessary. A more usual circumstance would involve the use of the fast BF_3 counter where the neutron flux density $\approx 10^3$ n/cm^2-sec time average. If the spill time is 100 msec, then the count rate will be about 10^5 counts/sec and the accumulated count will be $\approx 10^4$ counts/pulse with negligible loss.

We prefer that the pulses from the remote BF_3 system (detector, shaper, and line driver) be derived from linear circuits rather than from digital ones. Although very fast discriminator pulses can be generated at the detector, the nature of the signals that trigger the discriminator cannot be observed at the remote counting area.

An oscilloscope, set for single sweeps and triggered by the Bevatron beam-extractor timing pulse, is used to view a statistically significant number of single traces. The minimum time between two pulses on any single sweep is noted and compared with the pulse pair resolution time of the detector-counting system. Consecutive time segments along the entire duration of the beam spill can be inspected by using the delayed sweep facilities of the oscilloscope. The delay sweep is triggered by the beam extractor timing pulse. If the incidence of pulse pairs that approach the pulse pair resolution time is small, then counting losses will also be small. Methods similar to this are used to study neutron production during consecutive increments of time during the acceleration cycle by gating the various counters ON during this time.

Pulses from a paraffin-moderated enriched BF_3 detector (Anton No. 805, 20 cm Hg) are fed into a MOS source follower. Pulse shaping is accomplished by the 10-μH inductor in the source leg (see Fig. 7), and Q_2 and Q_3 are used in a low-output-impedance cascaded emitter-follower configuration. Overall sensitivity of the system is ≈ 2 counts/neutron-cm^2 on the flat portion of the discriminator curve (Fig. 9).

There will be a variety of rise times within the BF_3 tube. Those events which occur in regions of low electric field intensity will have the longest rise times. Figure 8 shows the pulse width at half-maximum amplitude of the largest pulses to be 30 nsec. Table 1 shows the approximate pulse widths relative to the maximum amplitude as seen at the output of 300 feet of RG-58/U. This length of cable attenuates the pulse amplitude by 30% but does not affect pulse shape to any great extent. RG-58/U represents a worst case; RG-63 has less attenuation.

The signal voltage across the 10-μH pulse shaper will depend on the rise time of the input pulse ($E_L = L \frac{dI}{dt}$), and as a result the pulse-height spectrum is weighted with small pulses. The extent to which this degrades the discriminator plateau and increases the gamma sensitivity was investigated. Figure 9 indicates that an adequate "plateau" does exist. Sensitivity to gamma radiation was checked by placing a 900-mg Ra source 4 cm from the center of the detector. The gamma level at that point was nearly 500 R/h, and the overall average is estimated to be about 200 R/h along the full length of the detector. With a discriminator setting of 20 mV the Ra source did not affect the count rate from a nearby neutron source. At a discriminator setting of 3 mV the gammas nearly jam the counter, but the count rate decreases rapidly at higher discriminator settings.

In addition to the fast output pulses there is provision for extracting positive-going 5-μsec-width pulses at the drain of Q_1 (Fig. 10). This is useful with slower amplifiers and scalers for those applications which do not require fast counting.

Table 1. Pulse width relative to maximum amplitude.

Fraction of maximum pulse height	Pulse width (nsec)
1	30
3/4	45
1/2	60
1/4	80

4π G-M ANTICOINCIDENCE FOIL COUNTER

This system was constructed to allow field counting of moderated neutron-activated indium and gold foils.[5] Figure 11 shows the equipment. The anticoincidence circuit is shown in Fig. 12.

Background with 2 in. Pb is 23 counts/min in each counter, while the anticoincidence background is 21 counts/min. The foil to be counted is placed on a thin Mylar membrane between the two counters. A 2-g 2-in.-diam indium foil will yield 21 counts/min per n/cm^2-sec at zero time and at saturation. It can be seen from Fig. 12 that when G-M_1 and G-M_2 are in coincidence, Q_1 and Q_2 both conduct so that the gate of Q_3 becomes positive and cuts off. This makes the source of Q_4 negative and Q_4 is driven further into cutoff. The two pulses from G-M_1 and G-M_2 which were added in Q_6 and Q_7 and routed to Q_4 cannot progress further because Q_4 is cut off. On the other hand, if either Q_1 or Q_2 does not receive a pulse, Q_3 remains conducting and Q_4 is barely cut off, allowing a pulse from Q_6 or Q_7 to turn on Q_4 and switch off Q_5. In the absence of G-M pulse, all the transistors are cut off except Q_3 and Q_5, and the current drain is 16 mA. Both coincidence and anticoincidence outputs are available.

The digital circuit shows another unique property of enhancement-mode MOS's. It is possible to direct-couple stages without the need for bias-shifting resistors.

RADIATION-EFFECTS MEASUREMENTS

A natural extension of the work on portable MOS ionization chambers was the use of similar instruments in fixed installations for beam monitoring, beam steering, or control of access to high-level target areas. Some information on radiation-induced damage to MOS's was necessary before these applications could be pursued.

At one time it was thought that these devices would not be easily damaged by radiation. A primary mechanism of radiation damage in bipolar transistors is the disruption of the periodicity of the crystal lattice. These radiation-induced defects in the lattice act as recombination centers for minority carriers. MOS's do not depend on minority carriers, so it was thought that they should be very radiation-resistant. This is not the case, as will be shown.

Static measurements of radiation-induced damage were made on a group of forty 2N3608's. One group was in the range of absorbed dose from 10^4 to 10^8 rads of 7.5-MeV electrons. A second group received 10^6 rads of 7.5-MeV (peak) bremsstrahlung gammas, and a third group received an integrated thermal neutron exposure of 4×10^{14} n/cm^2. All devices were irradiated under voltage.

The most significant change (see Fig. 13) was an upward shift in the gate-threshold or turn-on voltage, V_{GST}. This means that 15 V instead of 5 V are needed to turn the device on after absorbing 10^8 rads.

Changes in transconductance are of minor importance up to 10^8 rads. (See Fig. 14.) Gate leakage current becomes significantly higher at 10^7 rads, and at 10^8 rads I_G may increase by several orders of magnitude. (See Fig. 15.) I_{DSS} remains unchanged up to 10^6 rads. Beyond that, it increases an order of magnitude up to 10^8 rads. (See Fig. 16.) The breakdown voltages BV_{DSS} and BV_{GSS} were not affected.

CONCLUSION

MOS electrometers have many advantages to recommend them over vacuum-tube types. Among these are higher g_m, lower I_G, less drift, low current drain, and no filaments. They are more rugged and are free from rf interference. On the other hand, they are not nearly so radiation-resistant as vacuum tubes, and they must be well shielded if they are to be used in high-level radiation areas.

A moderated fast BF_3 counter capable of producing 30 to 80 ns pulse widths has been described. This allows sensitive BF_3 neutron detectors to be used where the neutron flux density is extremely high.

The 4π coincidence-anticoincidence G-M unit described is extremely simple and versatile. Either G-M unit can be read out individually, or the coincidence and anticoincidence pulses can be counted.

All the circuits are simple and straightforward, and most of the salient features of these devices have been demonstrated. Undoubtedly the amazing similarity between the MOS and the vacuum tube will suggest many other applications.

ACKNOWLEDGMENTS

The author wishes to thank the other members of the Health Physics Group, all of whom have helped in many different ways. In particular I wish to thank H. Wade Patterson, Alan Smith, and Lloyd Stephens for making sufficient time available and for their many suggestions and encouragements.

This work was done under auspices of the U. S. Atomic Energy Commission.

REFERENCES

1. Joseph B. McCaslin, Electrometer for Ionization Chambers Using Metal-Oxide-Semiconductor Field-Effect Transistors, Rev. Sci. Instr. 35 [11], 1587-1591 (1964).

2. Joseph B. McCaslin and James Carlyle, Some Radiation-Effects Measurements on Insulated-Gate Transistors, AEC Report UCRL-11936, Lawrence Radiation Laboratory, Mar. 1965.

3. General Micro-electronics, Inc., Santa Clara, California.

4. Alan R. Smith (Lawrence Radiation Laboratory), private communication.

5. Lloyd D. Stephens and Alan R. Smith, Fast-Neutron Surveys Using Indium-Foil Activation, AEC Report UCRL-8418, Lawrence Radiation Laboratory, Aug. 1958.

FIGURE CAPTIONS

Fig. 1. p-Channel metal-oxide-semiconductor. Negative gate-to-source voltage causes the silicon beneath the gate in the region on the silicon-quartz interface to become depleted of negative charge carriers. The remaining carriers are holes, so that there is a continuous p-type layer or p channel between source and drain. The conductivity of this p channel is modulated by the gate potential.

Fig. 2. Gate leakage current continues to decrease for several hours after turn-on.

Fig. 3. MOS integrating ionization chamber–rate meter has full-scale ranges of 1 and 10 μR and 1 mR/h to 10 R/h in decade steps. Input leakage current $\approx 10^{-16}$ A. The instrument exhibits freedom from drift and rf interference, also capability for continuous 7-month operation, and has low component cost.

Fig. 4. Schematic diagram of integrating ion chamber shows simplicity of balanced circuit. Q_2 compensates for temperature fluctuations and balances out quiescent current.

Fig. 5. Small MOS rate meter has full-scale decade ranges of 20 mR/h to 200 R/h, uses 125 cm^3 air ion chamber at 1 atmos.

Fig. 6. Moderated fast BF_3 detector with pulse shaper and line driver. When it is used with 300 ft RG-58/U, output pulses have a maximum amplitude of 220 mV. Pulse width depends on rise time, and will be 30 nsec for pulses of maximum amplitude and 80 nsec for 1/4-maximum-amplitude pulses.

Fig. 7. Fast BF_3 schematic: 10-μH inductance in Q_1 produces fast decay times, but also selectively attenuates slow-rising pulses. Q_2 and Q_3 drive the long cable. Positive-going pulses of 1.5 $V_{(max)}$ and of 5 μsec width are available at drain of Q_1, and can be used for slower counting work.

Fig. 8. Oscilloscope traces of maximum-amplitude fast BF_3 pulses at termination of 300 ft RG-58/U. Time base is 50 nsec/cm. These maximum-amplitude pulses also exhibit the fastest rise time (≈ 20 nsec) and consequently the shortest pulse width (≈ 30 nsec). Pulses of slower rise times, and reduced amplitudes, have pulse widths of about 80 nsec for pulses of 1/4 maximum amplitude.

Fig. 9. Discriminator plateau taken with moderated fast BF_3 counter. At an estimated gamma level of 200 R/h a very high count rate is obtained at a discriminator bias of 3mV; however, this diminishes very rapidly above 3mV and at 20 mV there is negligible effect.

Fig. 10. Provision exists at drain of Q_1 for positive-going BF_3 pulses of 1.5 V and of 5 μsec width. This is useful with slower amplifiers and scalers for those applications which do not require fast counting. Time base is 5 μsec/cm.

Fig. 11. 4π pancake G-M counters with 2-in. lead shield and coincidence-anticoincidence circuit. Large chassis is portable amplifier, scaler, and power supplies. System is used for field counting of moderated-neutron-activated gold and indium foils. Zero-time saturated activity from 2-in.-diam 2-g indium foil is 21 counts/min per n/cm^2-sec of PuBe neutrons. Anticoincidence background is 21 counts/min.

Fig. 12. Schematic of 4π G-M coincidence-anticoincidence circuit. In quiescent state, only Q_3 and Q_5 are conducting.

Fig. 13. Predominant effect of radiation damage to MOS's is the upward shift of the turn-on voltage V_{GST}. After receiving a dose of 10^8 rads, an MOS that previously needed only -5 V to turn on now needs -15 V.

Fig. 14. Radiation-induced changes in g_m are only of secondary importance.

Fig. 15. Gate leakage current increases considerably at 10^7 rads and is unpredictable at 10^8 rads.

Fig. 16. I_{DSS} begins to show a change at 10^6 rads and has increased by a factor of 10 at 10^8 rads.

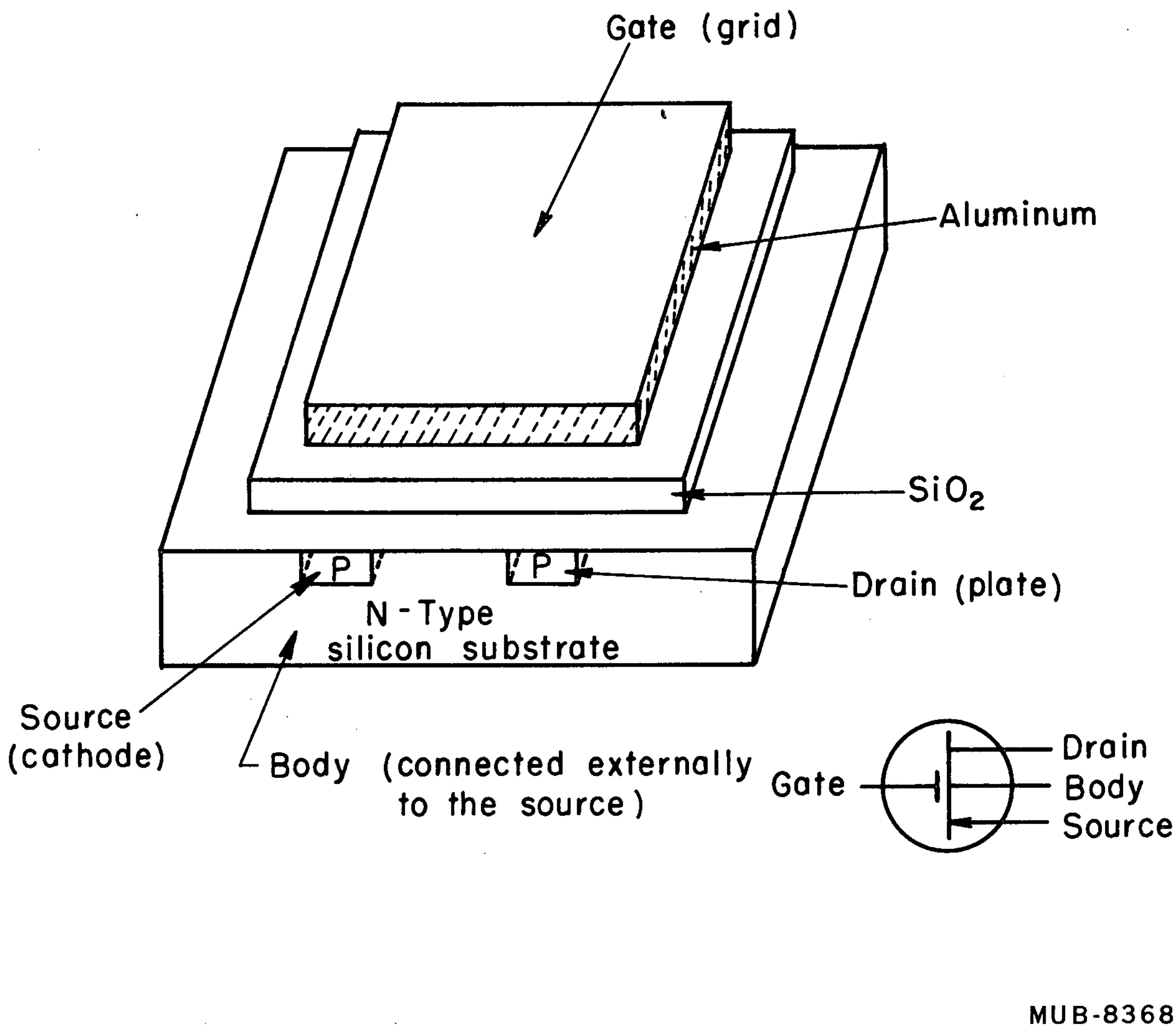
Gate (grid)
Aluminum
SiO_2
Drain (plate)
P
P
N-Type
silicon substrate
Source
(cathode)
Body (connected externally
to the source)
Gate
Drain
Body
Source
MUB-8368

Fig. 1

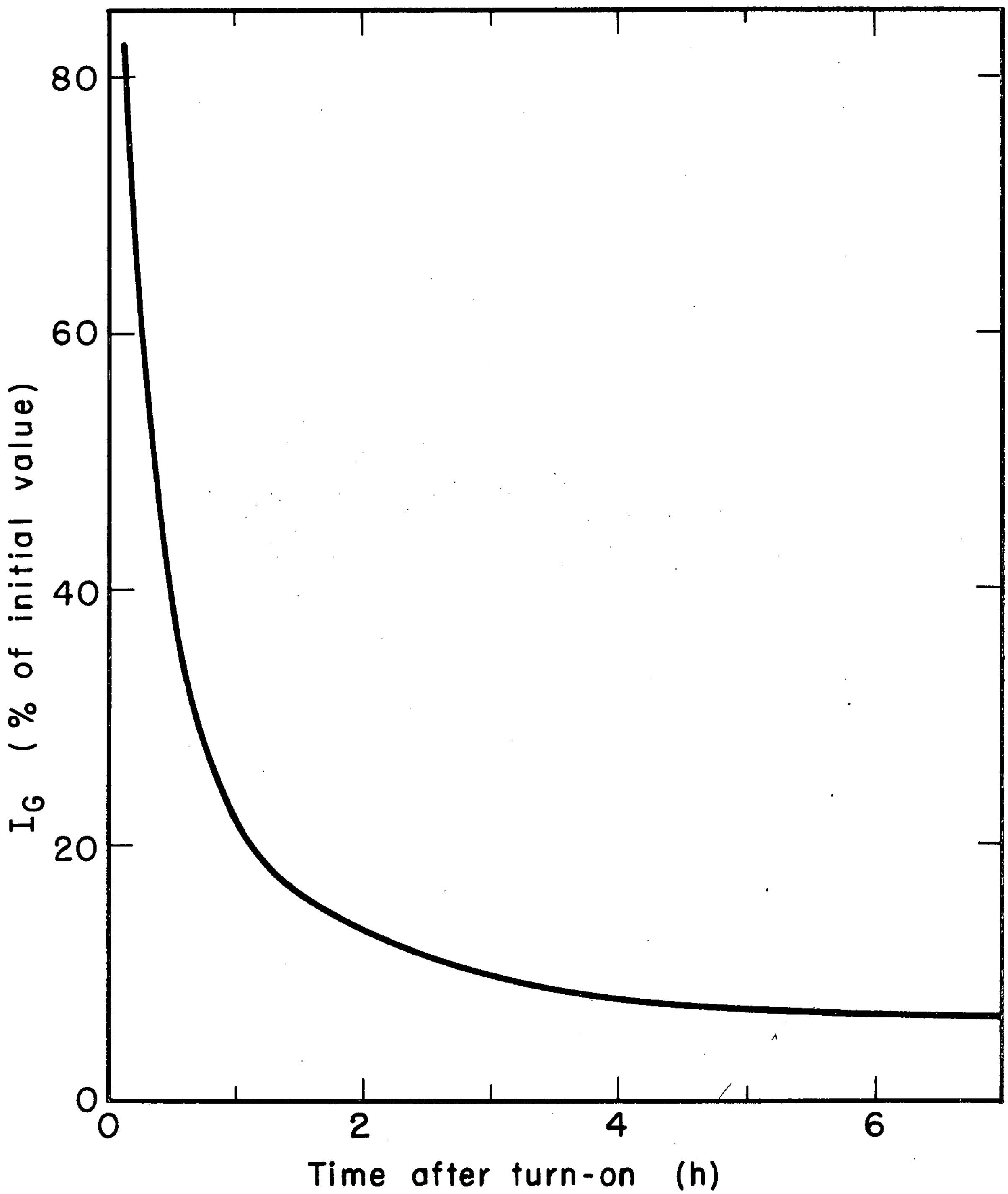

MUB-5650

Fig. 2

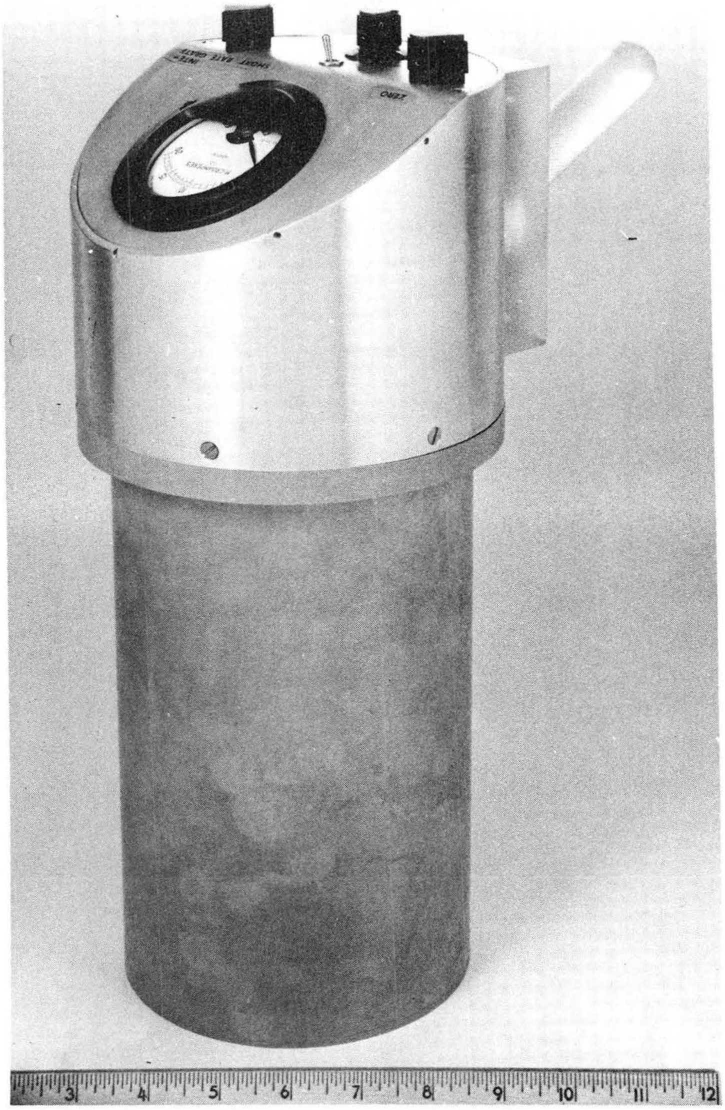

ZN-5203

Fig. 3

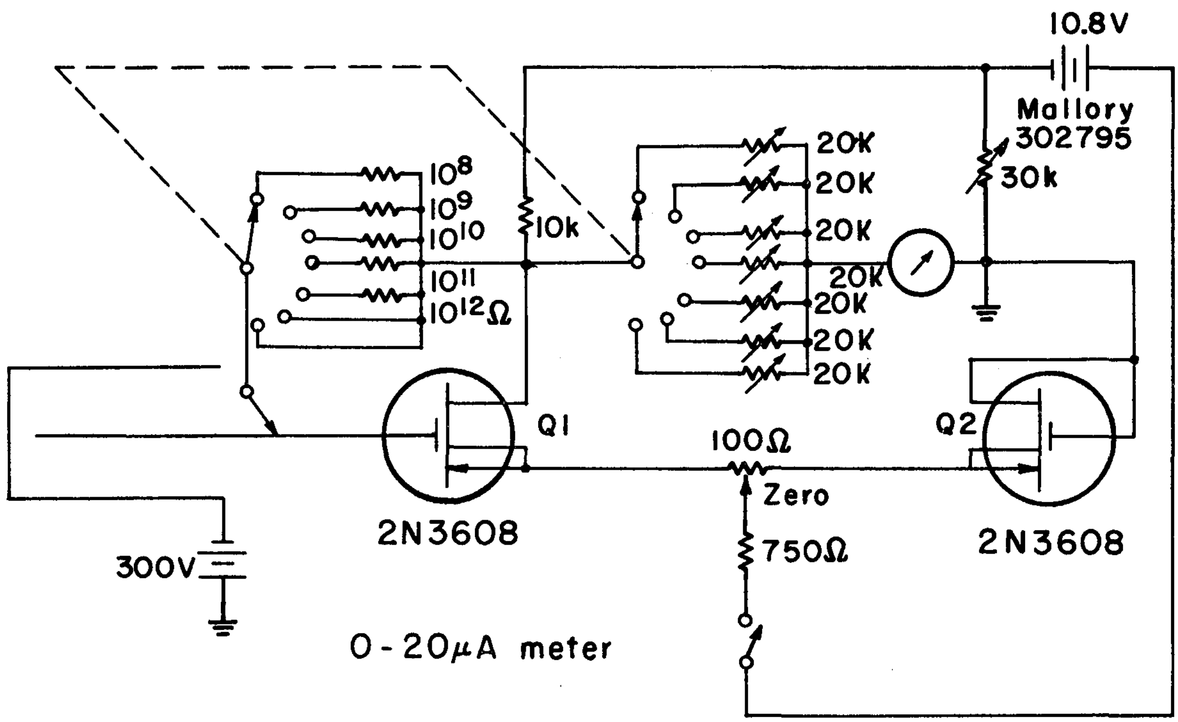
10.8V
Mallory 302795
30k
10k
10^8
10^9
10^{10}
10^{11}
$10^{12}\Omega$
20K
20K
20K
20K
20K
20K
20K
Q1
Q2
100Ω
Zero
750Ω
2N3608
2N3608
300V
0-20μA meter
MUB-8369

Fig. 4

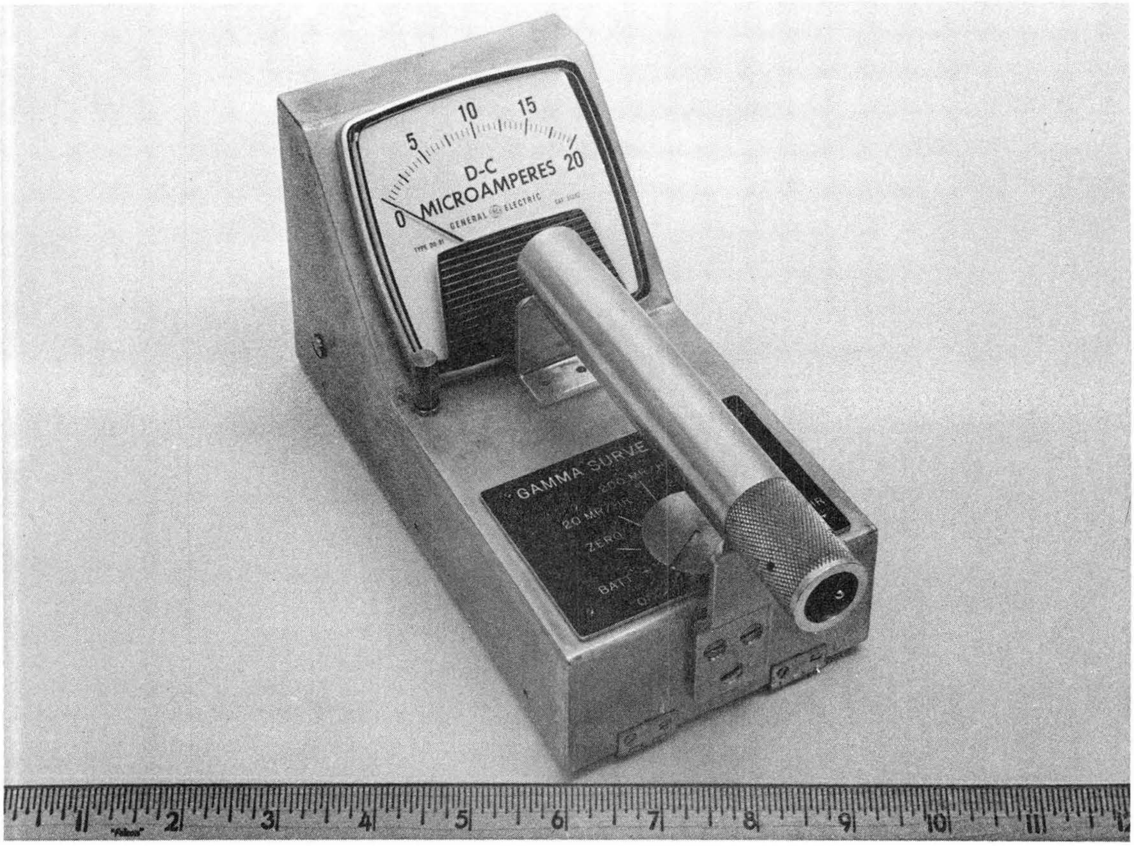
0
5
10
15
20
D-C
MICROAMPERES
GENERAL ELECTRIC
GAMMA SURVE
20 MR/HR
ZERO
BATT

ZN-5205

Fig. 5

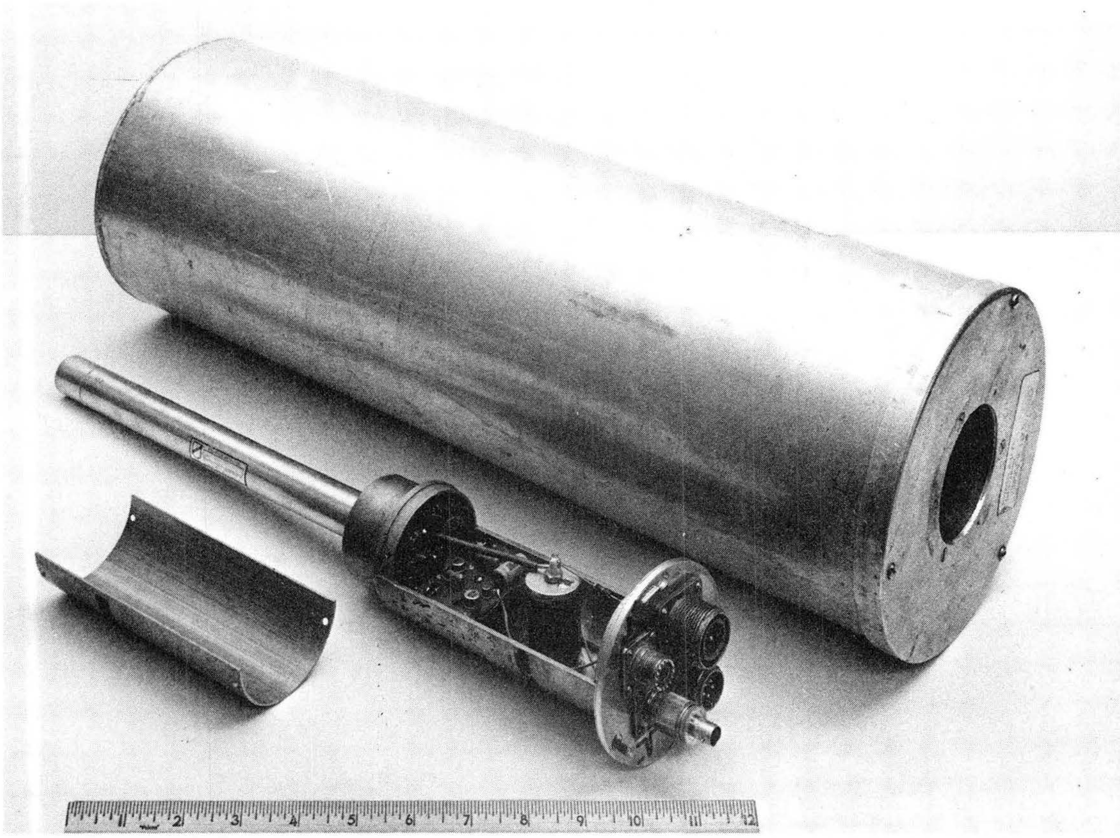

ZN-5206

Fig. 6

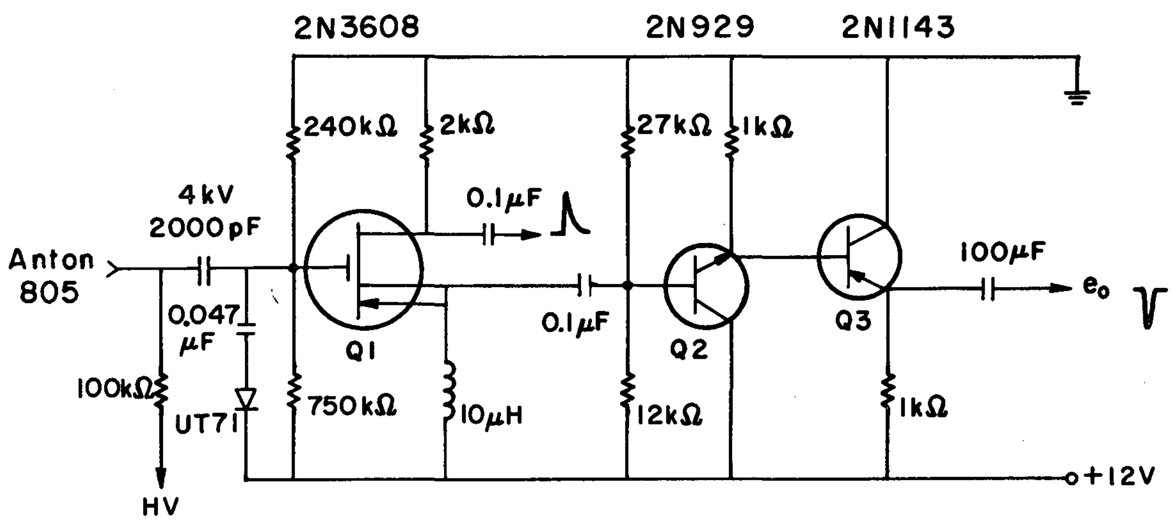

MUB-8370

Fig. 7

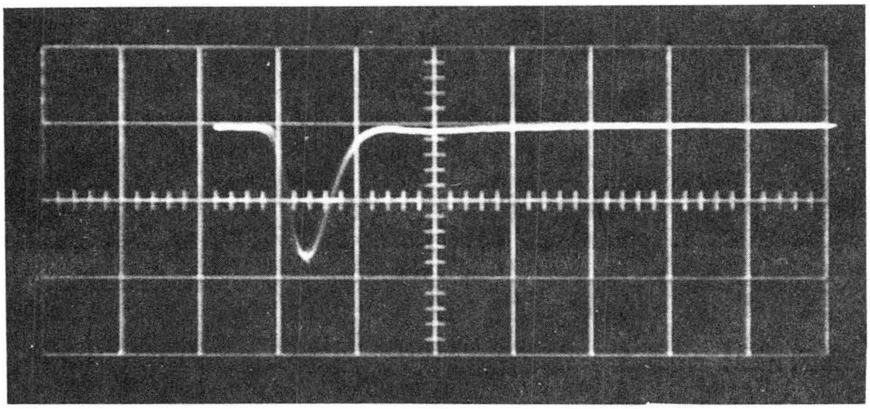

ZN-5201

Fig. 8

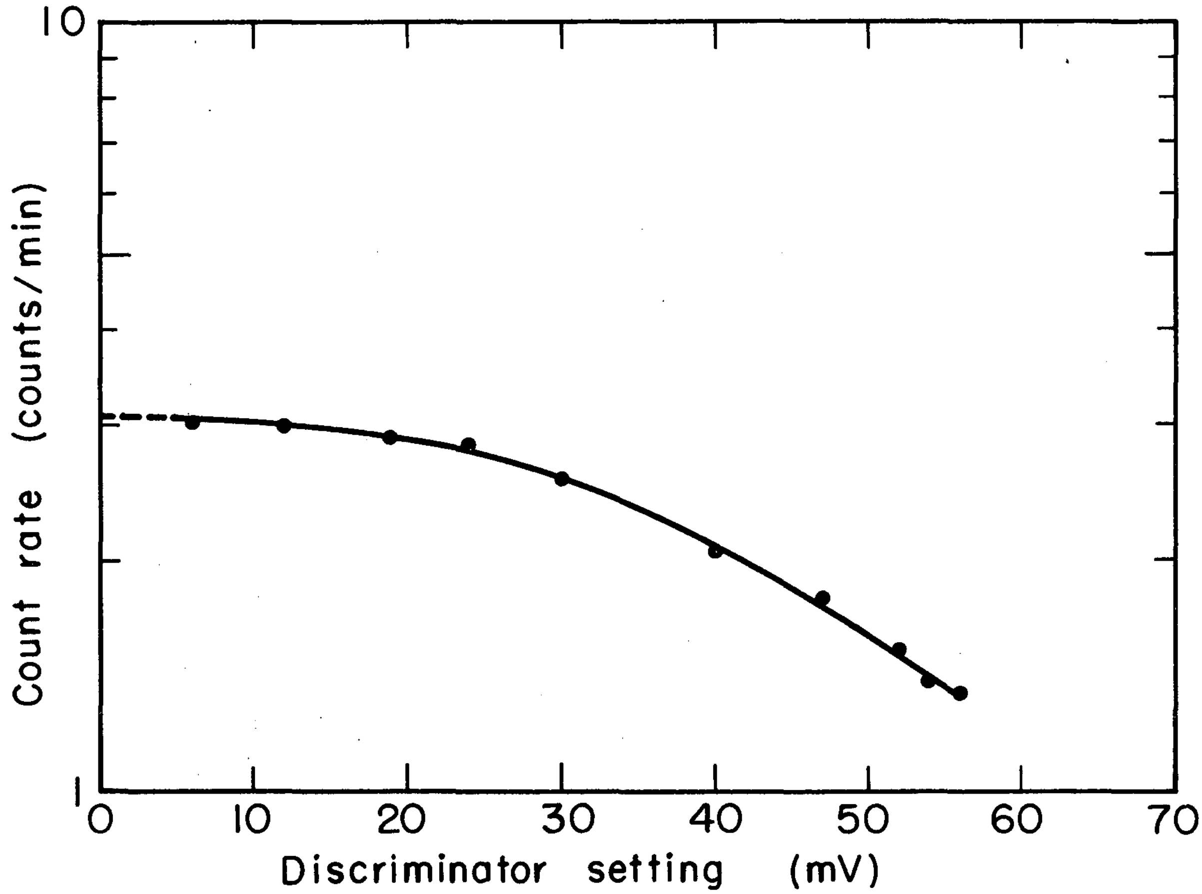

MUB-8371

Fig. 9

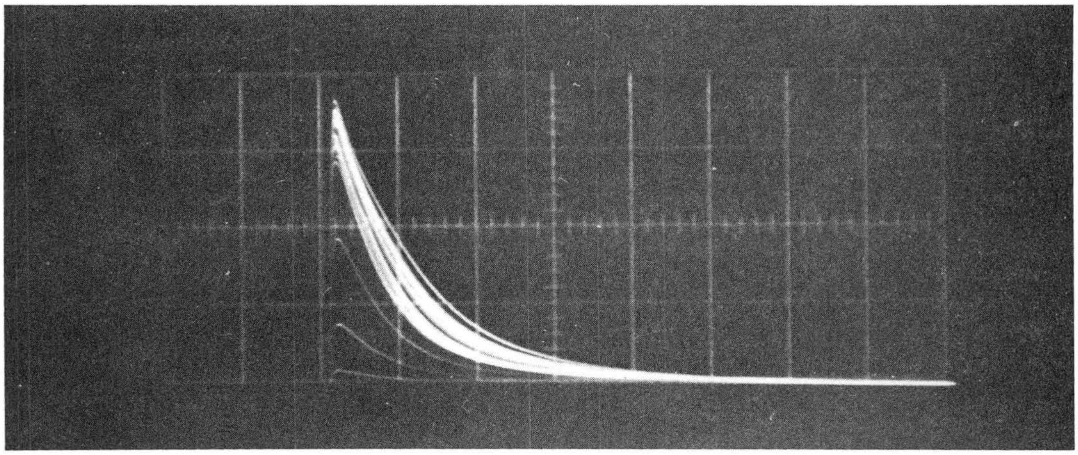

ZN-5202

Fig. 10

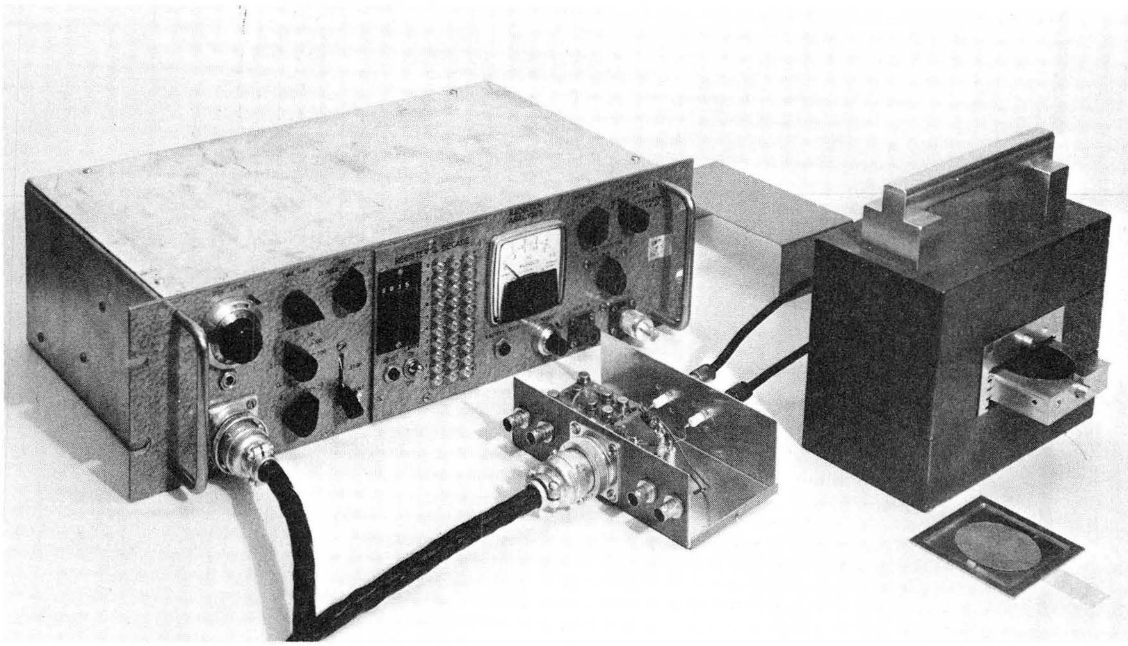

ZN-5207

Fig. 11

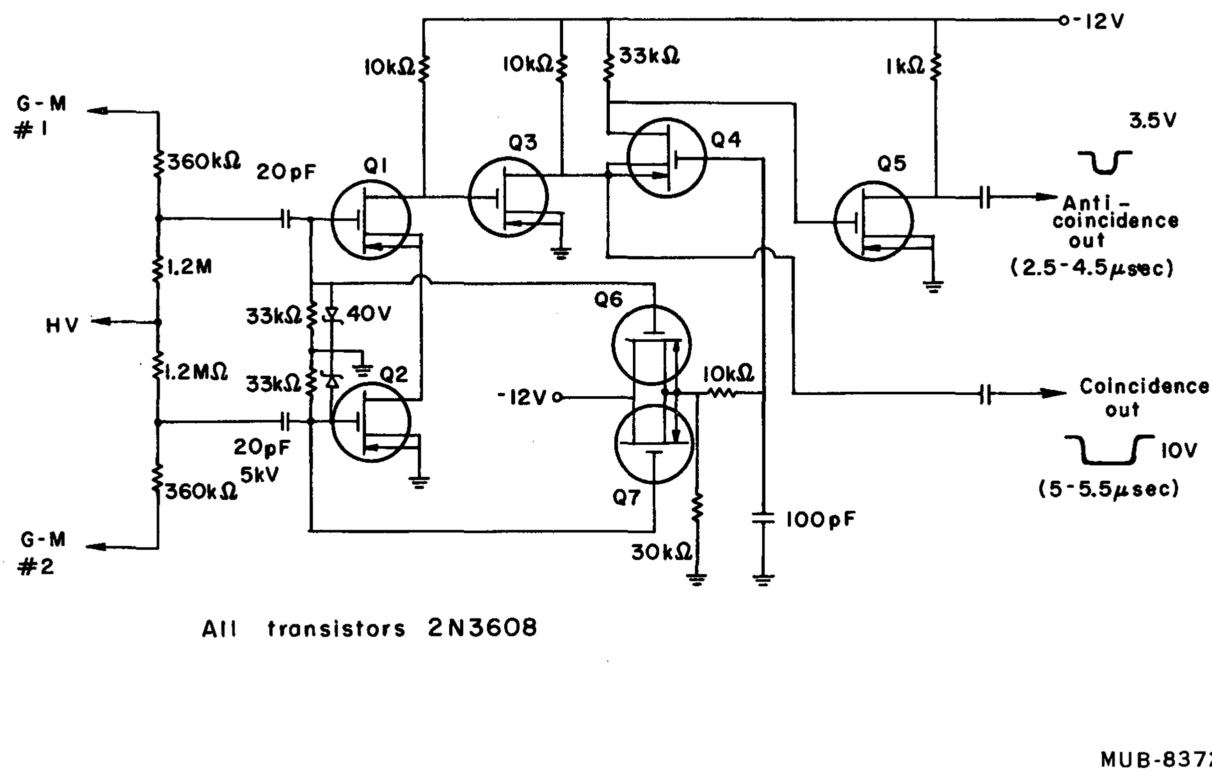
-12V
10kΩ
10kΩ
33kΩ
1kΩ
G-M
#1
360kΩ
20pF
Q1
Q3
Q4
Q5
3.5V
Anti-
coincidence
out
(2.5-4.5μsec)
1.2M
HV
33kΩ
40V
Q6
1.2MΩ
33kΩ
Q2
-12V
10kΩ
Coincidence
out
20pF
5kV
10V
(5-5.5μsec)
360kΩ
Q7
100pF
G-M
#2
30kΩ
All transistors 2N3608
MUB-8372

Fig. 12

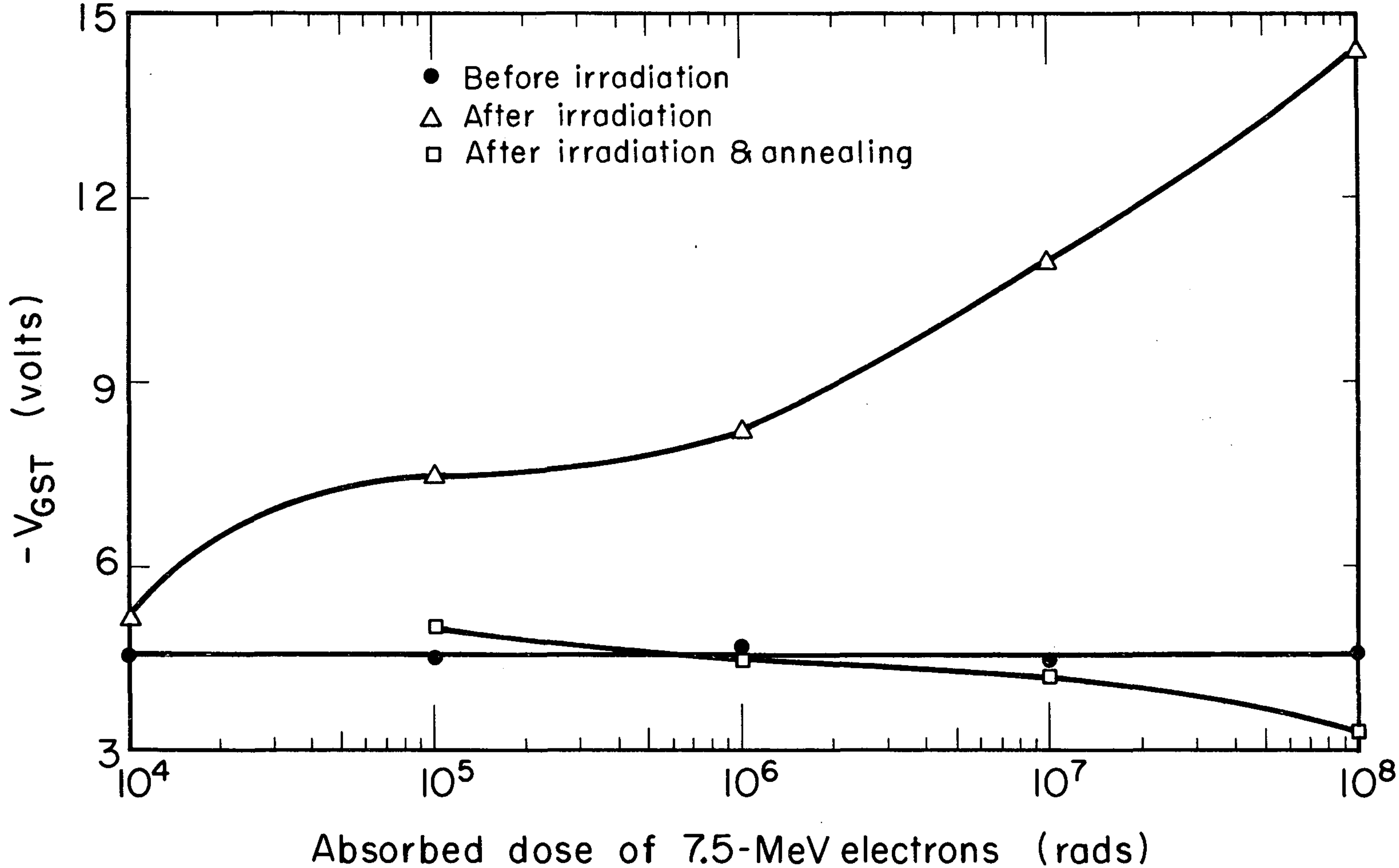

MUB-5655

Fig. 13

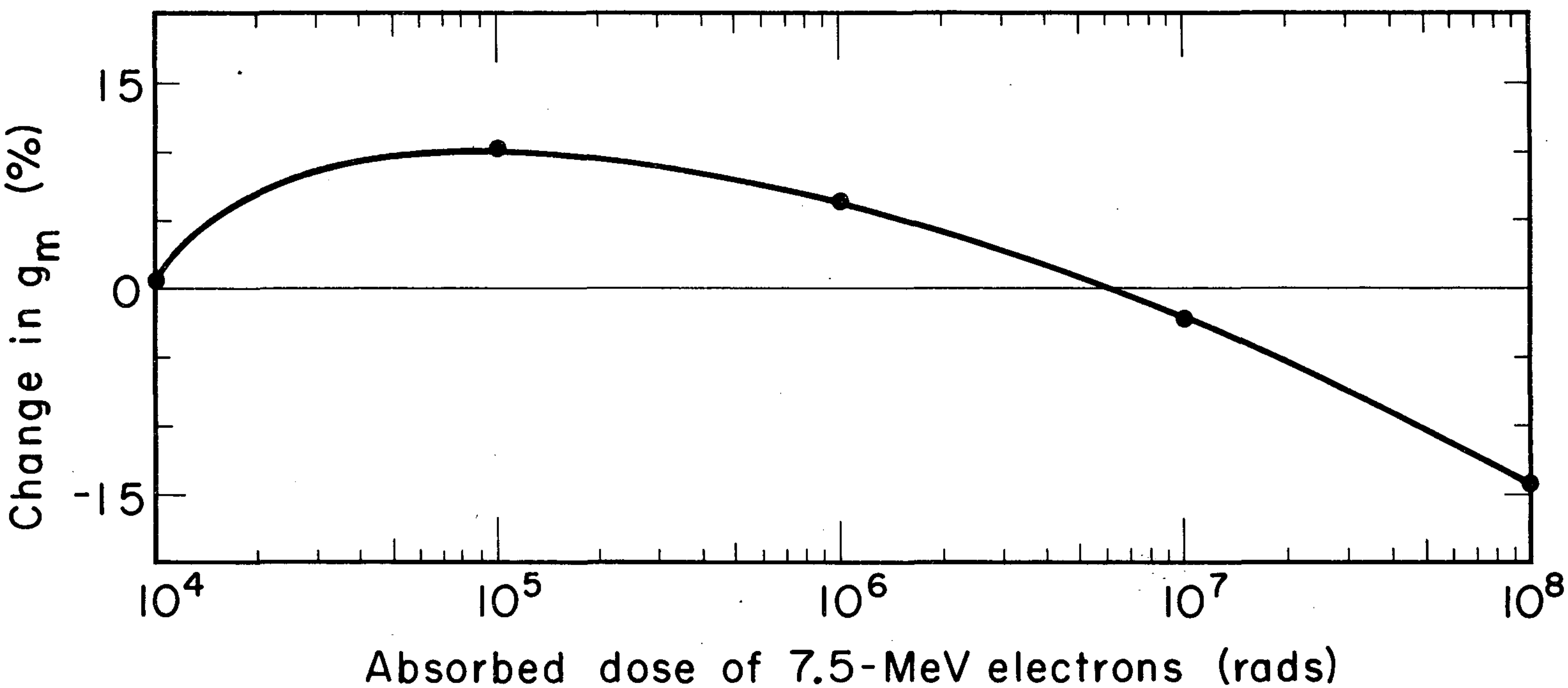

MUB-5652

Fig. 14

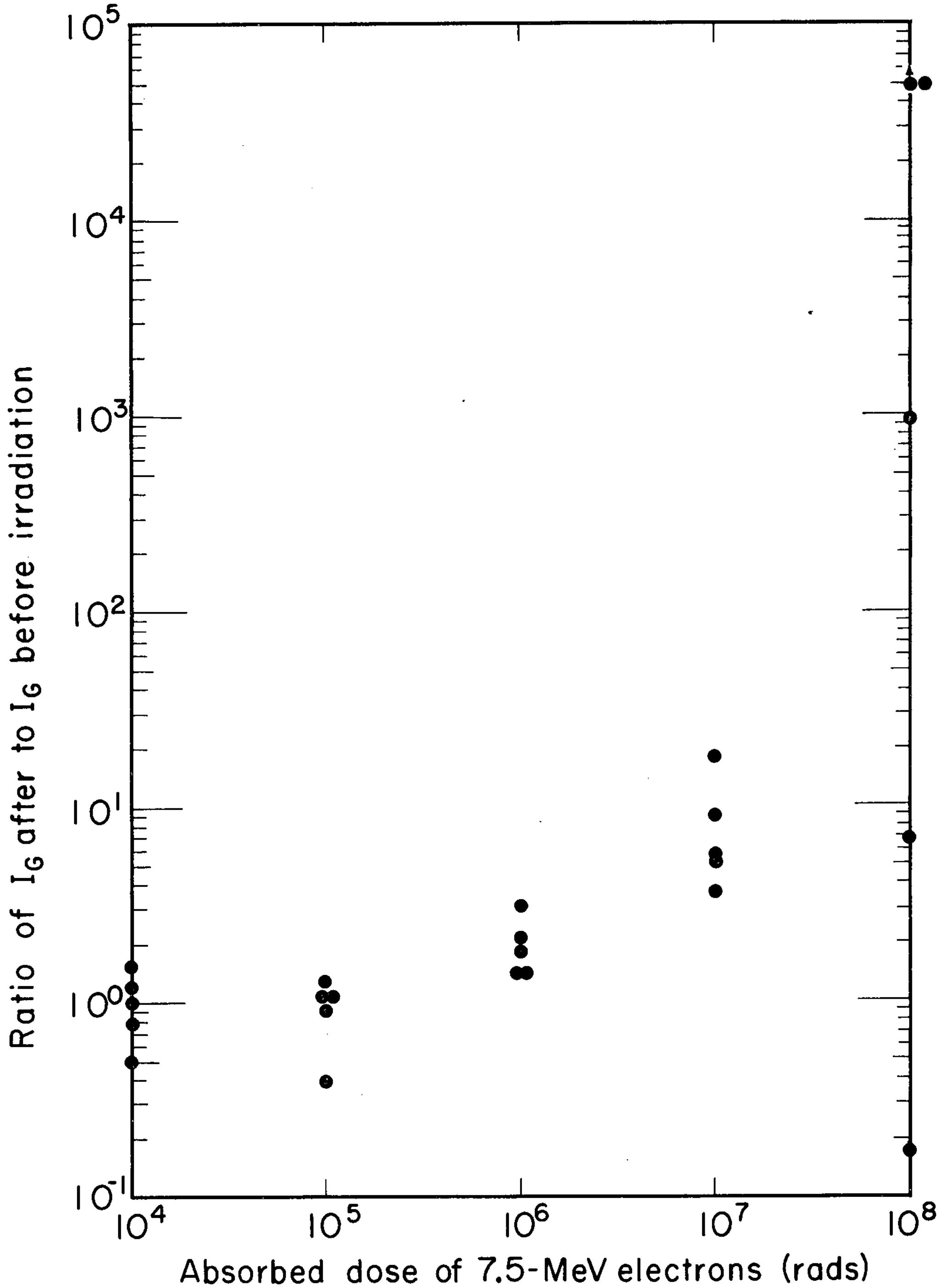

MUB-5653

Fig. 15

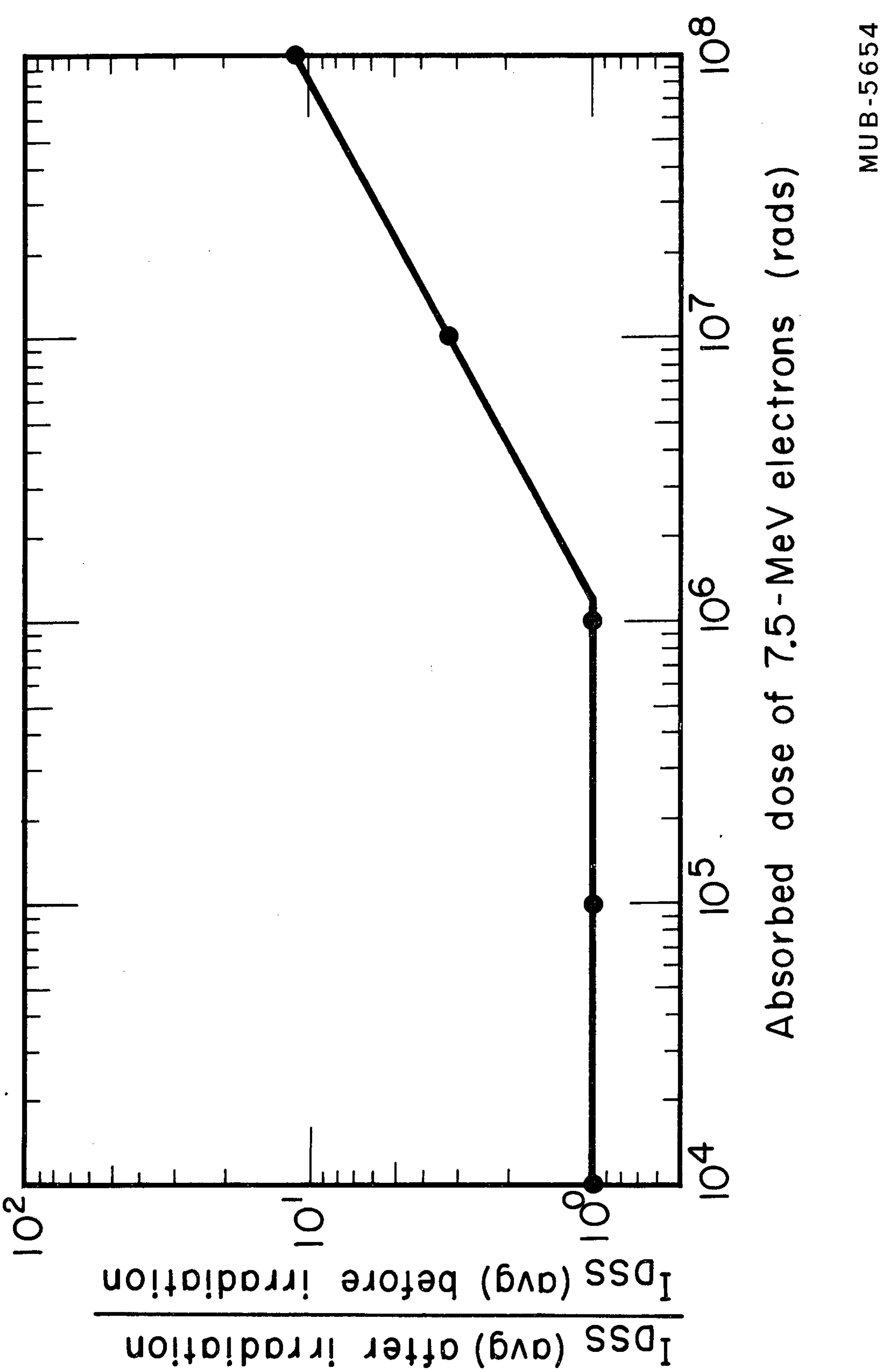

IDSS (avg) after irradiation / IDSS (avg) before irradiation
10^2
10^1
10^0
10^4
10^5
10^6
10^7
10^8
Absorbed dose of 7.5-MeV electrons (rads)
MUB-5654

Fig. 16